Journal of
Nanoscience and Nanotechnology
Vol. 8, 1–6, 2008

Effect of Surface Roughness on the Subsequent Growth of MgO Nanowires

Hyoun Woo Kim*, Seung Hyun Shim, and Jong Woo Lee

School of Materials Science and Engineering, Inha University, Incheon 402-751, Republic of Korea

We demonstrated the variation of product morphology by varying the underlying surface characteristics, which were controlled by predeposition annealing. The surface roughness of the underlying In_2O_3 layer affected the resultant product morphology, indicating that rougher substrate favored the formation of one-dimensional (1D) structures. The obtained MgO nanowires were a single-crystal cubic structure. The PL measurement with a Gaussian fitting exhibited visible light emission bands centered at 2.26 eV and 2.86 eV.

Keywords: Nanowires, MgO, Surface Roughness.

1. INTRODUCTION

Since the first discovery of carbon nanotubes (CNTs),[1] much technological and scientific excitement has been raised by the discovery of various forms of nanostructures.[2–4] Among them, one-dimensional (1D) structures including nanowires, nanorods, and nanobelts have attracted much attention since the last decade due to their unique properties and potential applications to nanoelectronics and optoelectronics. Magnesium oxide (MgO) is a typical wide-band-gap insulator, having found many applications as catalysis, additives in refractory, paint and superconductor products, and substrates for thin film growth.[5, 6] In particular, MgO whisker has recently been developed as an intensifier used in superconductive and spaceflight composite materials. Accordingly, many research groups have reported on the synthesis of 1D MgO nanostructures.[7–13] However, they generally studied from the viewpoint of preparation method and characterization.

The film growth is known to depend strongly on the characteristics of the underlying layers or substrates. Particularly, it has been known that properties of subsequently formed film were dependent on the surface roughness of underlying layer.[14–16] Although we expect that the substrate surface roughness will also affect nucleation and growth behavior of 1D nanostructures, to the best of our knowledge, there has been no report on that matter.

In the present communication, in order to investigate the effect of surface characteritics on the morphology of subsequently deposited materials, we have chosen MgO and In_2O_3 as deposit and underlying material, respectively. We have varied the surface roughness of the In_2O_3 layers by thermal annealing at various temperatures. With obtaining the MgO nanowires, we have investigated the structural and photoluminescence (PL) properties.

2. EXPERIMENTAL DETAILS

As a starting material, we used standard polished sapphire (0001) wafers. The sapphire substrate was cut into small pieces with dimensions of 20 mm × 20 mm, which was subsequently cleaned in acetone and then rinsed by deionized water. A schematic diagram of the MOCVD apparatus used in the present study was previously outlined.[17] Triethylindium (TEI) and O_2 were used as sources. Ar gas (99.999% purity) passed through the TEI bubbler maintained at 35 °C, being saturated with the TEI vapor. The In_2O_3 film was synthesized by supplying O_2 and Ar carrier gases, respectively, with the flow rate of 5 standard cubic centimeters per minute (sccm) and 20 sccm at 200 °C for 1 h. After the deposition of In_2O_3 films, samples were annealed in a vertical quartz tube furnace in air ambient at temperatures in the range of 400–800 °C for 20 minutes.

The synthesis process for MgO structures was carried out in a horizontal quartz tube. The MgB_2 powders were placed in the center of the chamber and the substrate Si chip was situated on their top with the In_2O_3-layered side downwards. During the experiment, the chamber was heated to a temperature of 900 °C and held for 1 h, with the ambient gas ($Ar+O_2$) being at a constant total pressure of 2 Torr. The typical percentage of O_2 and Ar partial pressure, respectively, were set to approximately 3 and 97%.

*Author to whom correspondence should be addressed.

RESEARCH ARTICLE

The surface roughness of In_2O_3 film was measured using atomic force microscopy (AFM; Digital Instruments Nanoscope III). The as-synthesized MgO films or nanowires were examined by grazing angle (0.5°) X-ray diffraction (XRD, Rigaku DMAX 2500) with CuKα_1 radiation ($\lambda = 0.154056$ nm) and scanning electron microscopy (SEM, Hitachi S-4200). TEM experiment was performed in a Philips CM-200 TEM operated at 200 kV, with energy-dispersive X-ray spectroscopy (EDX) attached. The PL measurement was carried out at room temperature by using a SPEC-1403 photoluminescence spectrometer with a He-Cd laser (325 nm, 55 mW).

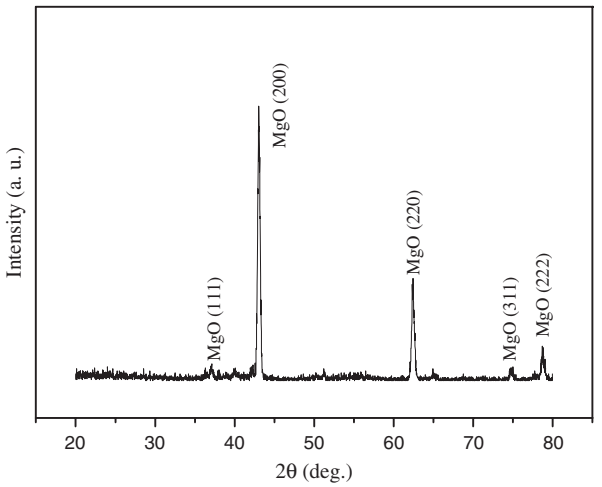

Fig. 1. XRD patterns of the final product with the predeposition annealing of In_2O_3 layers at 800 °C.

3. RESULTS AND DISCUSSION

Figure 1 indicates the XRD spectrum of the final product with the predeposition annealing of In_2O_3 layers at 800 °C. The diffraction peaks of (111), (200), (220), (311), and (222) correspond to the cubic MgO structure with a lattice constant of $a = 0.421$ nm (JCPDS: 04-0829). XRD analyses revealed that products were an MgO phase whether the predeposition annealing was performed or not and regardless of annealing temperature in the range of 400–800 °C.

Figure 2(a) shows the top-view SEM image of MgO structure deposited on the as-prepared In_2O_3 film. Although there rarely exists the 1D structure (as indicated by Arrow 1), the product mainly consists of the film-like structures (Arrow 2). Figure 2(b) represents an EDX spectrum associated with Figure 2(a), implying that the product corresponds to MgO, whilst Al, In and Pt peaks were originated from Al_2O_3 substrate, In_2O_3 layer, and SEM sample preparation, respectively. Figure 2(c) shows the SEM image of the MgO structure deposited on 400 °C-annealed In_2O_3 film, revealing that the product comprises bundles of 1D structures, as well as the film-like structures. The average diameter of the nanowires ranges from

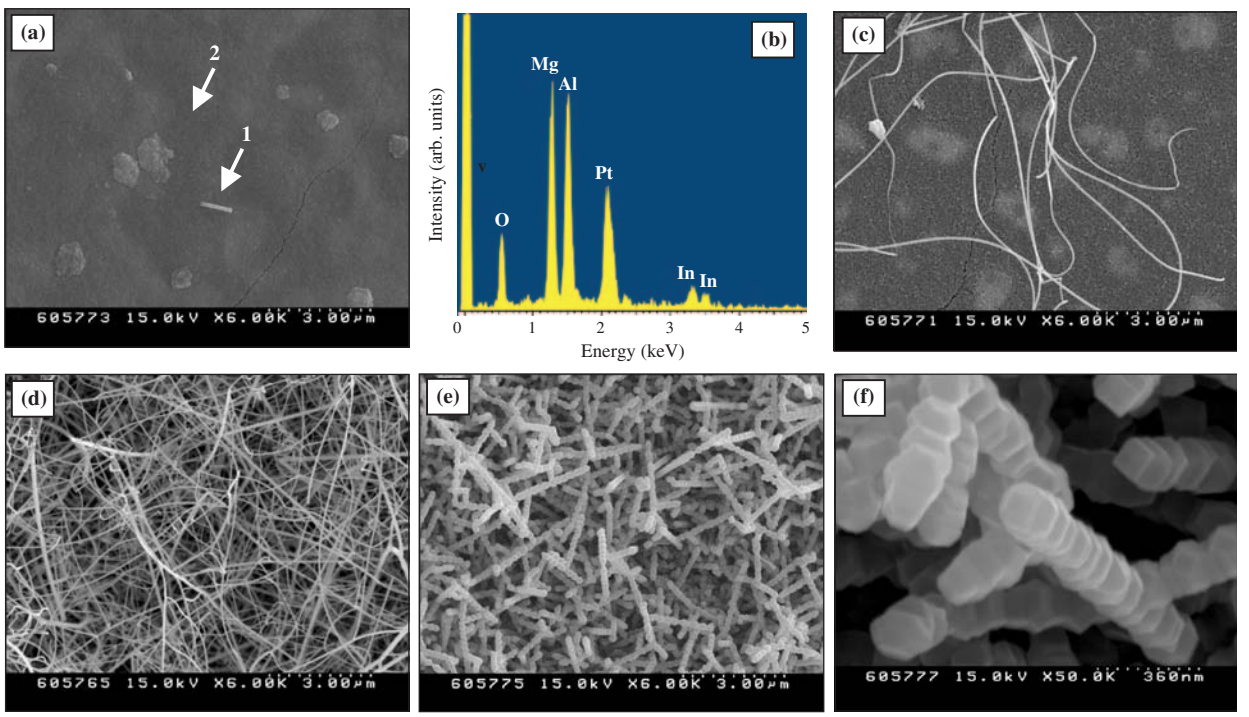

Fig. 2. Top-view SEM image of the final product (a) without a predepostion annealing and (b) corresponding SEM-EDX spectrum. Top-view SEM images of the final products with the predeposition annealing of In_2O_3 layers at (c) 400, (d) 600, and (e) 800 °C. (f) Enlarged SEM image corresponding to (e).

50 to 100 nm. Figures 2(d and e) indicate that both products deposited on 600 °C-annealed and 800 °C-annealed In_2O_3 films mainly consist of 1D structures. Figure 2(f) represents the enlarged image associated with Figure 2(e), revealing that there exists no nanoparticle at the tips of the 1D structures. Statistical analysis of many SEM images indicated that the average diameters of the 1D structures produced on 600 °C-annealed and 800 °C-annealed In_2O_3 films, respectively, were approximately in the range of 30–150 nm and 130–260 nm, suggesting that the average diameter of the 1D structures increased with increasing the annealing temperature in the range of 600–800 °C. From Figures 2(a, c, and d), we observe that the amount of 1D structures increases not only by carrying out the predeposition thermal annealing of In_2O_3 layers, but also by increasing the annealing temperature in the range of 400–600 °C.

In order to investigate the surface roughness of the In_2O_3 films, we have presented the AFM data. Figure 3(a) shows the AFM three-dimensional (3D) topography of the unannealed In_2O_3 film, whereas Figures 3(b, c, and d) show the AFM 3D topographies of the In_2O_3 films annealed at 400, 600, and 800 °C, respectively. The root mean square (RMS) roughness values of as-deposited, 400 °C-annealed, 600 °C-annealed, and 800 °C-annealed In_2O_3 layers are 3.4 nm, 6.4 nm, 23.2 nm, and 23.9 nm, respectively. Also, we estimated the horizontal distances between neighboring protrusions on the In_2O_3 layer surfaces (i.e., peak-to-peak distances) and Figures 4(a–d) show the surface topography images along the typical cross-section of the as-deposited, 400 °C-annealed, 600 °C-annealed, and 800 °C-annealed In_2O_3 layers, respectively. The average horizontal distances between the neighbouring protrusions were calculated to be approximately 45 nm, 49 nm, 63 nm, and 154 nm, respectively, for as-deposited, 400 °C-annealed, 600 °C-annealed, and 800 °C-annealed In_2O_3 layers. Therefore, in the present study, we reveal that RMS surface roughness and horizontal inter-protrusion distances coincidentally increases not only by employing the thermal annealing but also by increasing the annealing temperature.

AFM will measure a small region of the sample and the reading obtained may not always be the true surface roughness value for the complete coverage of the substrate. Actually, in the above analysis, we typically measured AFM data on the small region of 2 μm × 2 μm. Accordingly, we carried out AFM measurements in a wider substrate region of 20 μm × 20 μm. Figures 5(a, b, and c) represent the AFM 3D and cross-sectional topography images of annealed In_2O_3 films with an annealing temperature of 400 °C, 600 °C, and 800 °C, respectively. Although the difference in horizontal distances between the neighbouring protrusions cannot be noticeable due to relatively large area for AFM measurement, we reveal that RMS surface roughness increases by increasing the annealing

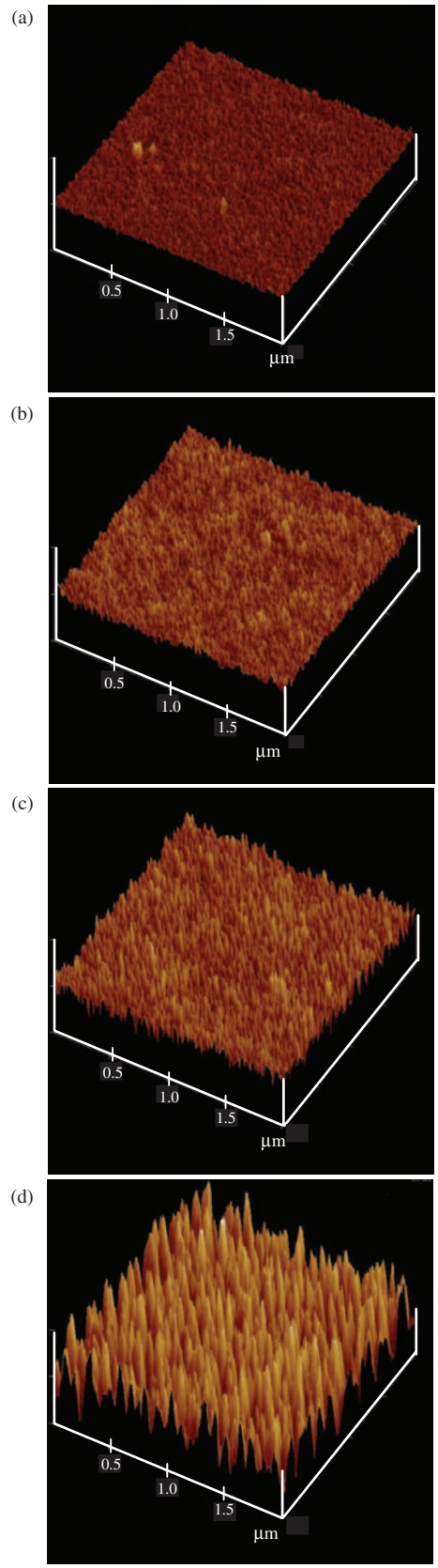

Fig. 3. AFM 3D images of (a) as-deposited In_2O_3 film and annealed In_2O_3 films with an annealing temperature of (b) 400 °C, (c) 600 °C, and (d) 800 °C.

RESEARCH ARTICLE

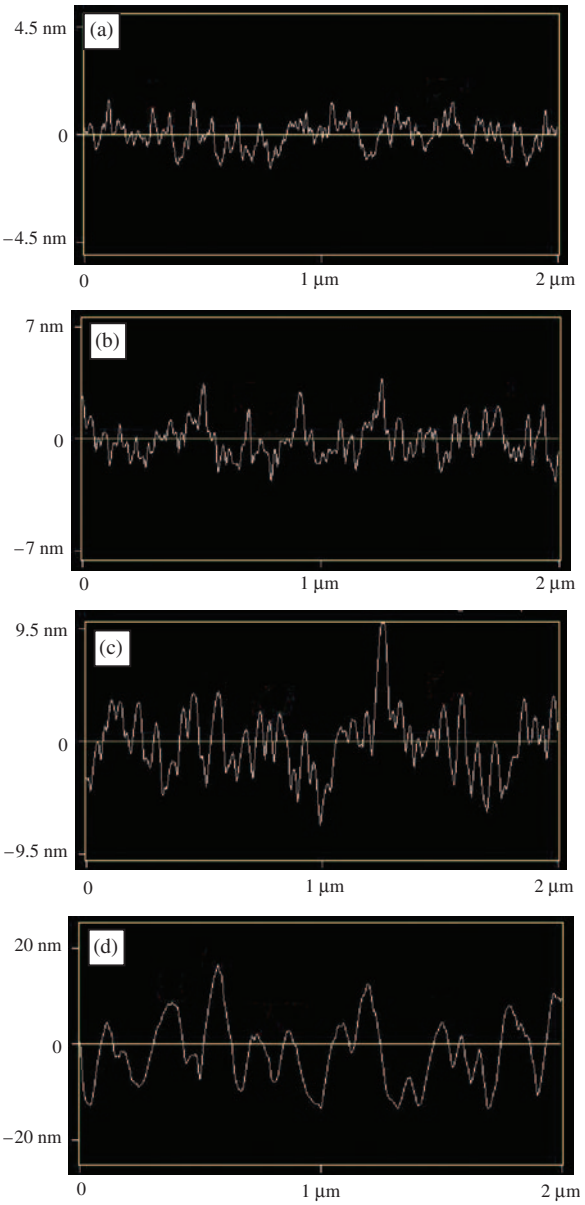

Fig. 4. AFM surface topography along the cross-section of (a) as-deposited In_2O_3 film and annealed In_2O_3 films with an annealing temperature of (b) 400 °C, (c) 600 °C, and (d) 800 °C.

temperature, agreeing with the AFM data from the smaller region of 2 μm × 2 μm.

From Figures 2 and 3, we suggest that the amount of 1D structures tends to increase with increasing the surface roughness of the underlying In_2O_3 layers, with the formation of MgO 1D structures being suppressed by employing a relatively flat In_2O_3 layer. Therefore, we suppose that the protruded or convex parts of the rough In_2O_3 layers provide the site for the independent growth of the 1D structure, whereas the relatively smooth In_2O_3 layer substrates with many nucleation sites promote the agglomeration of nuclei, ultimately producing cluster-like or film-like structures. In addition, sufficient horizontal inter-protrusion distance prevents agglomeration of nuclei, facilitating the independent growth of 1D structures. Furthermore, the larger horizontal distance may contribute to the generation of fewer nuclei per area, possibly increasing the nanowire diameter due to the concentrated flow of Mg and O elements towards a few nanowires for further growth (Figs. 2(d and e)). Similarly, our previous experiments indicated that the characteristics of underlying gold (Au) layer affected the morphology of the final MgO structures,[18] in which the intentionally formed Au islands provide the sites for the independent growth of the 1D structures.

For obtaining more detailed information about the individual MgO nanowires, we have carried out the TEM analysis. Figure 6(a) exhibits the TEM image of a single nanowire with the diameter of approximately 180 nm. Figure 6(b) shows an associated selected area electron diffraction (SAED) pattern. The SAED pattern can be indexed for [001] zone axis of crystalline MgO. The length direction is supposed to be along the [100] direction, as shown in Figure 6(a). Figure 6(c) is a high resolution TEM (HRTEM) image taken from the nanowire in Figure 6(a), revealing a good crystallinity. The interplanar spacings are about 0.21 nm, corresponding to the (200) and (020) planes of cubic MgO. EDX spectrum on the wire tip shows the signals of Mg and O elements, in addition to C elements from TEM grid (Fig. 6(d)). Accordingly, we reveal that the nanoparticle does not comprise an additional metal element. In the present work, since no metal has been intentionally used and SEM and TEM-EDX analyses provided no evidence that the catalyst was present at the tips of the 1D structures, the growth mechanism of MgO 1D nanostructures cannot be ascribed to the VLS mechanism, where the metal catalyst particles act as a liquid-forming agent. Instead, this type of growth is likely to be attributed to the VS mechanism, in which the Mg vapor generated from the MgB_2 powders combines with oxygen vapor, ultimately forming solid MgO nanowires.

The PL spectrum of the MgO nanowires at room temperature is shown in Figure 7. In order to have more closer insights for the origin of emission, we have fitted the spectral feature with Gaussian functions. The best fit of the emission was obtained with two Gaussian functions, with peaks being centered at 2.26 and 2.86 eV, respectively. First, there exists a green emission band peaked at an energy of 2.26 eV, which corresponds to the wavelength of 550 nm. Similarly, intensive green light emission from MgO nanobelts has been previously reported;[19] second, a blue emission band centered at around 2.86 eV (435 nm). The similar blue light emission has been previously observed from MgO nanostructures.[20, 21] Both blue and green light emissions may be associated with defects in MgO, including oxygen vacancy,[22] Mg vacancies and interstitials. The defects induce the formation of new energy levels in the band gap of MgO, contributing to the

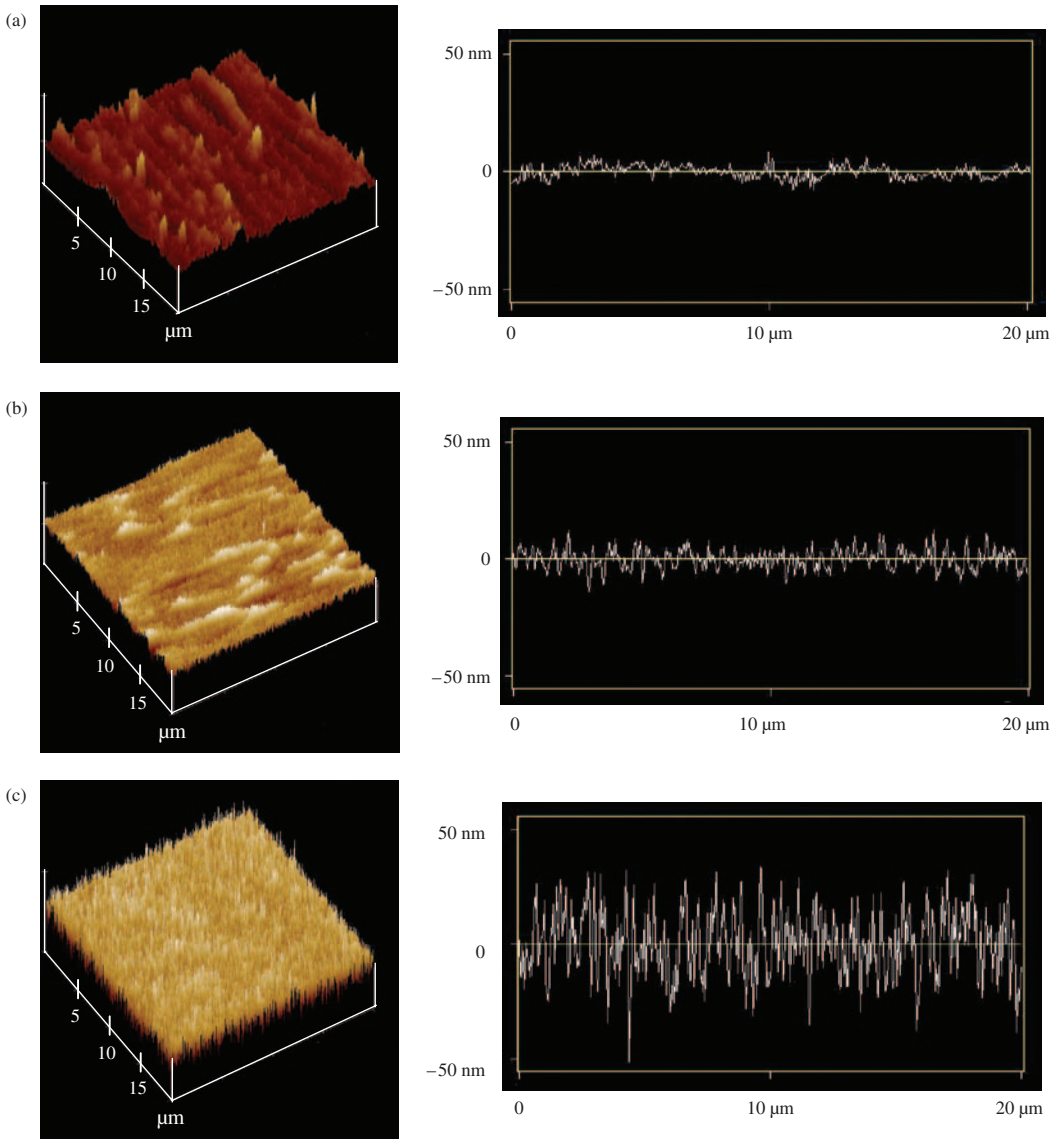

Fig. 5. AFM 3D (left-hand side) and cross-sectional (right-hand side) topographies of annealed In_2O_3 films with an annealing temperature of (a) 400 °C, (b) 600 °C, and (c) 800 °C, in a typical substrate region of 20 μm × 20 μm.

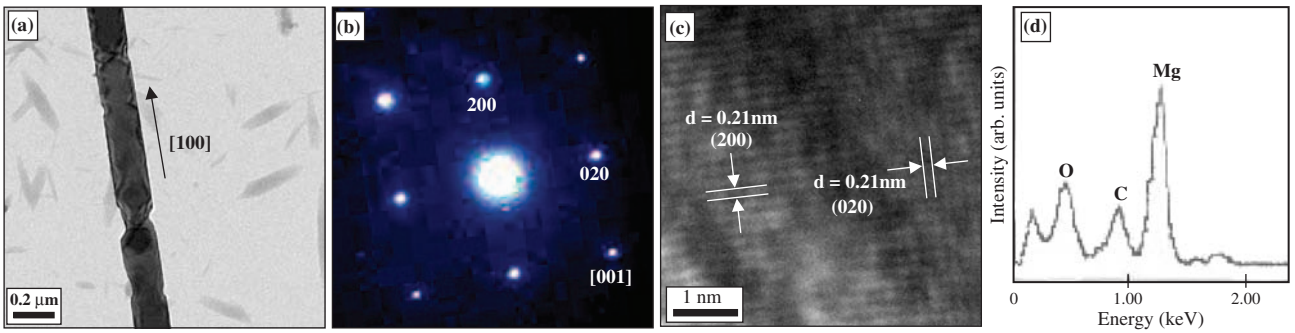

Fig. 6. (a) Low magnification TEM image of an MgO nanowire deposted on 800 °C-annealed In_2O_3 films. (b) Corresponding SAED pattern recorded along the [001] zone axis. (c) HRTEM image associated with the nanowire in (a). (d) TEM-EDX spectrum from the tip part of a nanowire. The C component has originated from the C-coated TEM grid.

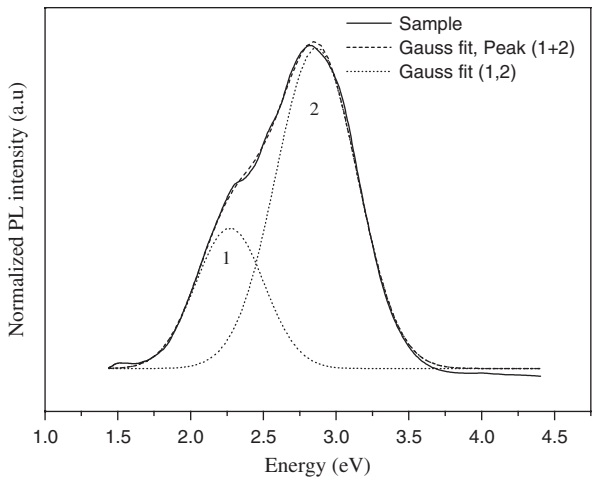

Fig. 7. Room-temperature PL spectrum of MgO nanowires upon a photoexcitation of 3.82 eV.

observed visible emission. In the present study, high temperature evaporation may have generated various defects.

4. CONCLUSION

By varying the surface characteristics of underlying In_2O_3 layers, we have fabricated MgO nanowires. The predeposition annealing of In_2O_3 layers at a sufficiently high temperature is necessary for large-scale production of nanowires. AFM images reveal that the thermal annealing at higher temperature helps to increase the RMS surface roughness and the horizontal distances between the neighbouring protrusions of the In_2O_3 layers. We have discussed the possible relationship between deposit morphology and underlying surface characteristics. The obtained MgO nanowires are crystalline, being likely to be attributed to a VS process. The PL measurement with the Gaussian fitting shows apparent visible light emission bands centered at 2.26 eV and 2.86 eV.

Acknowledgments: This work was supported by Inha University Research Grant.

References and Notes

1. S. Iijima, *Nature* 354, 56 **(1991)**.
2. C. B. Murray, C. R. Kagan, and M. G. Bawendi, *Science* 270, 1335 **(1995)**.
3. J. Hu, T. W. Odom, and C. M. Lieber, *Acc. Chem. Res.* 32, 435 **(1999)**.
4. Z. W. Pan, Z. R. Dai, and Z. L. Wang, *Science* 291, 1947 **(2001)**.
5. R. Z. Ma and Y. Bando, *Chem. Phys. Lett.* 370, 770 **(2003)**.
6. Y. Q. Zhu, W. K. Hsu, W. Z. Zhou, M. Terrones, H. W. Kroto, and D. R. M. Walton, *Chem. Phys. Lett.* 347, 237 **(2001)**.
7. P. D. Yang and C. M. Lieber, *Science* 273, 1836 **(1996)**.
8. Y. Q. Zhu, W. K. Hsu, W. Z. Zhou, M. Terrones, H. W. Kroto, and D. R. M. Walton, *Chem. Phys. Lett.* 347, 337 **(2001)**.
9. Y. Li, Y. Bando, and T. Sato, *Chem. Phys. Lett.* 359, 141 **(2002)**.
10. Y. Yin, G. Zhang, and Y. Xia, *Adv. Funct. Mater.* 12, 293 **(2002)**.
11. J. Zhang, L. Zhang, X. Peng, and X. Wang, *Appl. Phys. A* 73, 773 **(2001)**.
12. K. L. Klug and V. P. Dravid, *Appl. Phys. Lett.* 81, 1687 **(2002)**.
13. P. Yang and C. M. Lieber, *J. Mater. Res.* 12, 2981 **(1997)**.
14. S. H. Kim, S. W. Na, N.-E. Lee, Y. W. Nam, and Y.-H. Kim, *Surf. Coat. Tech.* 200, 2072 **(2005)**.
15. C. Y. Chan, S. Eyhusen, X. M. Meng, I. Bello, S. T. Lee, C. Ronning, and H. Hofsass, *Diam. Relat. Mater.* 15, 55 **(2006)**.
16. G. P. Singh, J. Alphonsa, P. K. Barhai, P. A. Rayjada, P. M. Raole, and S. Mukherjee, *Surf. Coat. Tech.* 200, 5807 **(2006)**.
17. H. W. Kim and N. H. Kim, *Appl. Phys. A* 81, 763 **(2005)**.
18. H. W. Kim and S. H. Shim, *Chem. Phys. Lett.* 422, 165 **(2006)**.
19. J. Zhang and L. Zhang, *Chem. Phys. Lett.* 363, 293 **(2002)**.
20. F. L. Deepak, P. Saldanha, S. R. C. Vivekchand, and A. Govindaraj, *Chem. Phys. Lett.* 417, 535 **(2006)**.
21. K. P. Kalyanikutty, F. L. Deepak, C. Edem, A. Govindaraj, and C. N. R. Rao, *Mater. Res. Bull.* 40, 831 **(2005)**.
22. G. H. Rosenblatt, M. W. Rowe, G. P. Williams, Jr., R. T. Williams, and Y. Chen, *Phys. Rev. B* 39, 10309 **(1989)**.

Received: 11 December 2006. Accepted: 10 April 2007.

RESEARCH ARTICLE